RSC Applied Interfaces

ROYAL SOCIETY OF CHEMISTRY

PAPER

View Article Online
View Journal | View Issue

Cite this: *RSC Appl. Interfaces*, 2025, **2**, 822

Thickness-induced metal–semiconductor transition in LaH_2 epitaxial thin films grown by reactive rf magnetron sputtering†

Sumireno Uramoto,[a] Hideyuki Kawasoko, *[bc] Satoru Miyazaki[a] and Tomoteru Fukumura [ad]

Received 28th October 2024,
Accepted 8th March 2025

DOI: 10.1039/d4lf00367e

rsc.li/RSCApplInter

Rare-earth hydrides have been extensively studied for their metal–insulator transition, high-temperature superconductivity and high hydride ionic conduction. Hence, research on their thin films is of great interest for exploring future-/next-generation device applications. In this study, (111)-oriented LaH_2 epitaxial thin films with varying thicknesses were grown for the first time *via* reactive rf magnetron sputtering. In the thicker films, the out-of-plane and in-plane lattice spacings were almost similar to those of bulk LaH_2. As the thickness decreased, the out-of-plane lattice spacing increased significantly, probably due to lattice strain, while the in-plane lattice spacing increased slightly. The thicker films exhibited metallic behavior similar to bulk LaH_2, whereas the thinner films were narrow band-gap semiconductors with a direct transition, indicating a thickness-induced metal–semiconductor transition without altering the hydrogen composition. These results suggest that strain engineering of rare-earth hydrides could enable the control of their physical properties even under ambient conditions.

Introduction

Rare-earth hydrides have been widely studied for their interesting physical properties, such as electrochromic switchable mirrors and near-room-temperature superconductivity under high pressure.[1–5] High hydride ion conduction in rare-earth hydrides has attracted much attention for its electrochemical implications in battery applications.[6–8] Complex rare-earth hydrides are also anticipated to serve as a platform for exploring novel physical properties.[9–11] Owing to these interesting properties, recent studies have also focused on thin film growth to expand the range of applications for various rare-earth hydrides.[12–16]

Fluorite-type LaH_2, which consists of a face-centered-cubic (fcc) La lattice with tetrahedral sites occupied by H atoms, is known to possess a metallic band structure due to the $5d^1$ electron configuration of the divalent La ion.[17] The metallic ground state of LaH_2 has been confirmed through specific heat and magnetic susceptibility measurements at low temperatures using polycrystalline bulk specimens.[18,19] Regarding the electrical conduction of LaH_2, superconductivity has been reported in polycrystalline bulk specimens, although clear experimental evidence, such as zero resistance, has not been demonstrated. In addition, recent theoretical calculations have predicted superconductivity in LaH_2 due to the rearrangement of H atoms into the interstitial octahedral sites of the fcc La lattice in fluorite-type LaH_2.[20] Additionally, a LaH_2 monolayer with a hexagonal lattice has been predicted to be a direct semiconductor.[21] Therefore, it is of interest to evaluate the intrinsic electrical conduction of LaH_2 at low temperatures using single crystalline specimens, such as epitaxial thin films. However, LaH_2 has so far been synthesized as polycrystalline bulks and thin films by heating La metal with a Pd capping layer in a hydrogen atmosphere[1,2,15–17,19–25] or, more recently, through a mechanochemical approach.[26] In addition, rare-earth hydrides, such as LaH_2, are unstable in air, making it difficult to synthesize single-phase specimens free of impurities.[9,18,21]

Recently, rare-earth hydride thin films have been directly grown using new approaches, such as pulsed laser deposition or reactive sputtering, without the need for a Pd capping layer.[9] For example, single-phase YH_2 epitaxial thin films have been successfully synthesized by reactive rf magnetron sputtering.[11] By using an *in situ* grown capping layer, the stability of the YH_2 films in air has been improved, resulting in higher electron mobility than polycrystalline bulk YH_2.[11]

[a] *Department of Chemistry, Graduate School of Science, Tohoku University, Sendai 980-8578, Japan*
[b] *Department of Chemistry, Graduate School of Science, Tokyo Metropolitan University, Hachioji 192-0397, Japan. E-mail: kawasoko@tmu.ac.jp*
[c] *PRESTO, Japan Science Technology Agency, Saitama 332-0012, Japan*
[d] *Advanced Institute for Materials Research (WPI-AIMR), Tohoku University, Sendai 980-8577, Japan*

† Electronic supplementary information (ESI) available. See DOI: https://doi.org/10.1039/d4lf00367e

In this study, (111)-oriented LaH_2 epitaxial thin films were synthesized for the first time by reactive rf magnetron sputtering with an *in situ* grown SiN_x capping layer. The out-of-plane lattice spacing increased significantly as the thickness decreased, suggesting the presence of thickness-dependent lattice strain. From electrical resistivity and optical absorption spectroscopy, the thicker films exhibited metallic behavior similar to bulk LaH_2, while the thinner films were semiconductors, a behavior not previously reported for bulk LaH_2. These results indicate a thickness-induced metal–semiconductor transition, probably attributed to lattice strain.

Experimental

LaH_2 (111) epitaxial thin films with varying thicknesses (38–121 nm) were grown on CaF_2 (111) single crystal substrates by reactive rf magnetron sputtering using an La metal target at a substrate temperature of 300 °C in an Ar/H_2 mixed gas atmosphere with a pressure of 0.02 Torr (H_2 concentration: 3.6%) and a typical deposition rate of 1.1 nm min^{-1}. Subsequently, SiN_x (5 nm) thin films were grown *in situ* on the LaH_2 (111) epitaxial thin films as a capping layer by rf magnetron sputtering using a SiN_x target at room temperature (~25 °C) in the same gas pressure. The thickness of the films was measured by X-ray reflectivity measurement (D8 DISCOVER, Bruker AXS). The crystal structure was evaluated by X-ray diffraction (XRD) using Cu Kα radiation (D8 DISCOVER, Bruker AXS; SmartLab, Rigaku). The chemical composition was evaluated using hydrogen forward scattering spectrometry (HFS) and Rutherford backscattering spectrometry (RBS), which were non-destructive analysis methods that did not require removal of the SiN_x capping layer to prevent film degradation. The surface morphology was observed using an atomic force microscope (SPI4000, Hitachi High Technologies). Electrical resistivity was evaluated using the van der Pauw method with a physical property measurement system (PPMS, Quantum Design). The absorption spectra were evaluated from the transmittance and reflectance spectra at room temperature (~20 °C) using a Fourier transform infrared spectrometer (FT/IR-6600, JASCO) and an ultraviolet-visible-near-infrared spectrometer (V-770, JASCO).

Results and discussion

Fig. 1a shows the X-ray diffraction patterns of the thin films. In all the thin films, only the 111 and 222 diffraction peaks of LaH_2 were observed, in addition to the diffraction peaks of the CaF_2 substrate, representing the single-phase nature of LaH_2 in the films. The full width at half maximum (FWHM) of the diffraction peaks for the LaH_2 epitaxial thin films decreased as the film thickness increased (Fig. S1†). This trend is reasonably explained using the Debye–Scherrer equation, which represents the relationship between the FWHM and the film thickness. No diffraction peak corresponding to the SiN_x phase was observed, indicating the amorphous nature of the capping layer. Fig. 1b and c show the depth profile of the chemical composition for the thin films, including the SiN_x capping layers and CaF_2 substrates, as measured by RBS and HFS. For the 39 nm-thick film (Fig. 1b), Si and N were homogeneously distributed near the surface up to a depth of 5 nm, corresponding to the SiN_x capping layer. From a depth of 5–40 nm, only La and H were homogeneously distributed, with an atomic ratio of H/La of 2.15, corresponding to the LaH_2 thin film. Above 40 nm, only Ca and F signals were homogeneously distributed, corresponding to the CaF_2 substrate. This depth profile

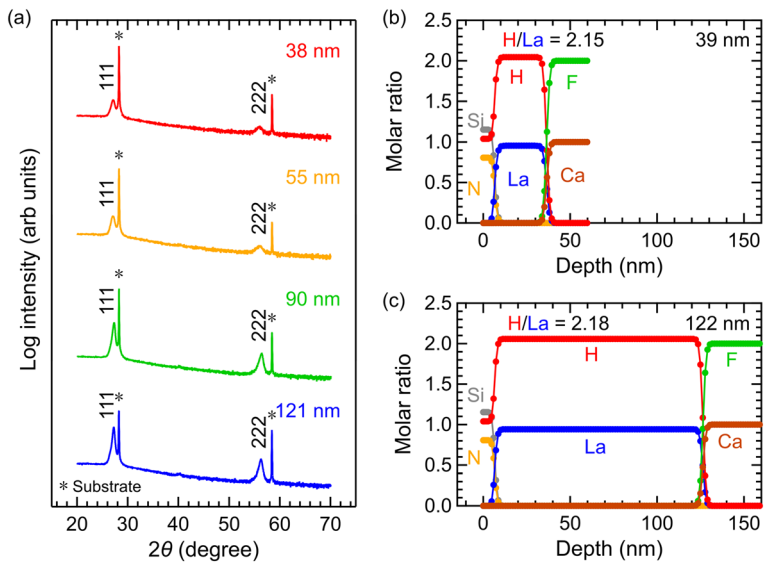

Fig. 1 (a) 2θ–ω X-ray diffraction patterns of LaH_2 epitaxial thin films with different film thicknesses. Depth profiles of the chemical composition of the (b) 39- and (c) 122 nm-thick LaH_2 films with SiN_x capping layers grown on CaF_2 substrates. The zero depth corresponds to the surface of the SiN_x capping layer.

confirmed negligible atomic diffusion between the SiN_x capping layer, the LaH_2 thin film, and the CaF_2 substrate. Similarly, the 122 nm-thick film showed negligible atomic diffusion at each interface, with La and H homogeneously distributed from 5–125 nm, maintaining an atomic ratio of H/La of 2.18 (Fig. 1c). These results indicated that the chemical composition of the thin films remained approximately the same regardless of their thickness. It was noted that the H/La ratio greater than 2 suggested the presence of excess H at the interstitial octahedral sites in the fluorite-type LaH_2. For LaH_2 thin films, the root mean square roughness was approximately 1.0 nm (Fig. S2†), indicating good surface flatness independent of thickness. Additionally, the crystal domain size was found to be approximately 100 nm.

Fig. 2a–d show the reciprocal space mappings near the 311 diffraction of LaH_2 thin films with different thicknesses. For all the thin films, the LaH_2 311 diffraction appeared as a spot shape, representing the epitaxial growth of LaH_2 thin films with the in-plane orientation of $LaH_2[11{-}2]//CaF_2[11{-}2]$. As the thickness increased, the Q_x and Q_z values of the LaH_2 311 diffraction peak decreased, indicating thickness-dependent lattice strain.

Fig. 3 shows the relationship between the lattice spacings of d_{111} and d_{11-2} for LaH_2 epitaxial thin films with different thicknesses. Both d_{111} and d_{11-2} were calculated from the LaH_2 311 diffraction peak in the reciprocal space mappings (Fig. 2a–d), corresponding to the lattice spacings along the out-of-plane and in-plane directions (see the inset of Fig. 3), respectively. Both d_{111} and d_{11-2} were the shortest for the 123 nm-thick film. For thicknesses down to 55 nm, the d_{111} remained almost constant at around 0.326 nm, while the d_{11-2} slightly increased. Both d_{111} and d_{11-2} for the 55-, 90-, and 123 nm-thick films were similar to those of bulk $LaH_{2.15}$ and $LaH_{2.18}$. However, the d_{111} of the 42 nm-thick film significantly increased compared to the thicker films,

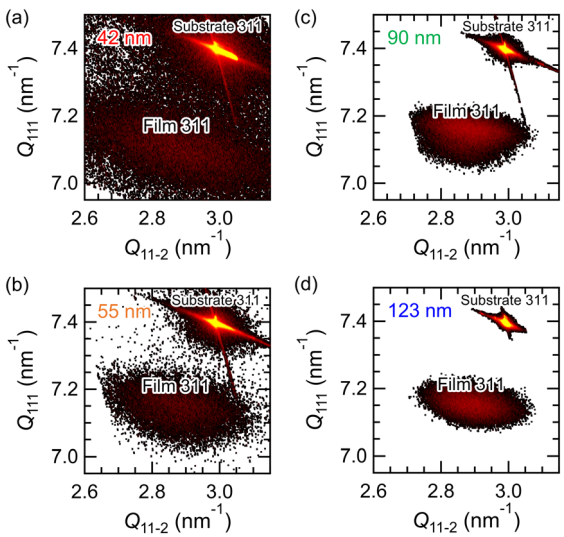

Fig. 2 (a)–(d) Reciprocal space mappings near the 311 diffraction for LaH_2 epitaxial thin films with thicknesses of (a) 42, (b) 55, (c) 90, and (d) 123 nm.

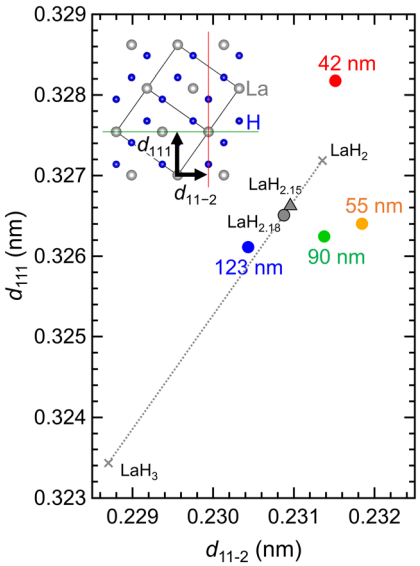

Fig. 3 Lattice spacings of (111) and (11–2) planes, denoted by d_{111} and d_{11-2}, respectively, for LaH_2 epitaxial thin films with different thicknesses. Gray circles and triangles denote the d_{111} and d_{11-2} of bulk $LaH_{2.15}$ and $LaH_{2.18}$, respectively, which are calculated from the lattice parameters of bulk LaH_2 and LaH_3 using Vegard's law.[31,32] Gray crosses denote the d_{111} and d_{11-2} of bulk LaH_2 and LaH_3.[31,32]

while the d_{11-2} remained similar to that of the thicker films. These results indicated that the d_{111} was largely modulated as a function of thickness compared to the d_{11-2}. The large elongation of d_{111}, reproducibly observed for different thin films (Fig. S3†), could be attributed to lattice strain, probably due to the smallest thickness, since all these films had almost the same chemical composition. From first-principles calculations of the bulk modulus (77.5 GPa) and Poisson's ratio (0.285) for LaH_2,[27] the out-of-plane strain was estimated to be approximately 1 GPa (Fig. S4†). Such significant strain effects were achieved despite a relatively large lattice mismatch of 3.7%, which could be a unique characteristic of hydrides. The origin of the lattice strain was unlikely to be simple epitaxial strain, as the lattice mismatch between CaF_2 and LaH_2 was as large as 3.7%. Moreover, it was unlikely that these strain effects were caused by the heating or cooling processes during thin film growth, since the thermal expansion coefficients of LaH_2 and CaF_2 were comparable.[28,29] Thus, the origin of the lattice strain could be domain matching epitaxy due to the shared fluorite-type structure of LaH_2 and CaF_2.[30]

Fig. 4a shows the temperature dependence of the electrical resistivity for the LaH_2 epitaxial thin films. The 121 nm-thick film showed the lowest electrical resistivity with a metallic temperature dependence, *i.e.*, positive $d\rho/dT$, consistent with the metallic ground state of LaH_2. The electrical resistivity at room temperature of the 121 nm-thick film (600 μΩ cm) was higher than that of bulk LaH_2 (30 μΩ cm).[1] As the thickness decreased, the electrical resistivity increased monotonically, and the 38 nm-thick film exhibited a semiconducting temperature dependence,

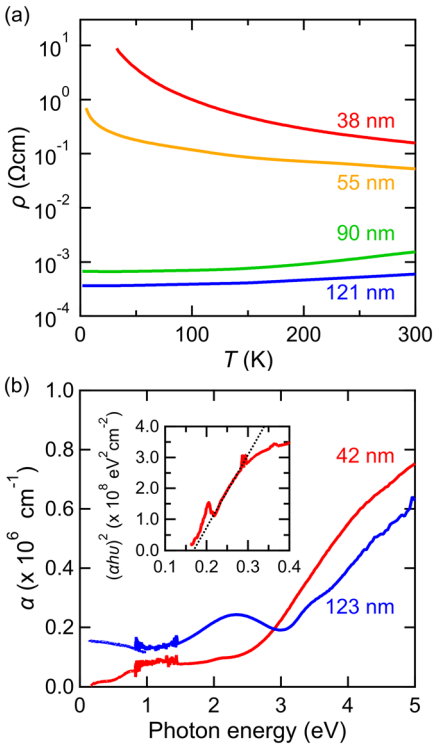

Fig. 4 (a) Temperature dependence of electrical resistivity and (b) optical absorption spectra for LaH_2 epitaxial thin films with different thickness. The inset of (b) shows the Tauc plot of the absorption edge, where the dotted line denotes the fitting line to evaluate the band gap.

i.e., negative dρ/dT, while the 55 nm-thick film showed a small hump around 230 K (Fig. S5†). Fig. 4b shows the optical absorption spectra for the LaH_2 epitaxial thin films. The 123 nm-thick film showed no absorption edge, indicating the metallic ground state. The absorption peak at 2.2 eV was also observed in a previous study, attributed to interband absorption for La.[33] However, the 42 nm-thick film showed an absorption edge around 0.1 eV, consistent with the semiconducting behavior observed in the electrical resistivity of the 38- and 55 nm-thick films (Fig. 4(a)). The Tauc plot of the absorption edge indicated a direct band gap of 0.17 eV for the 42 nm-thick film (inset of Fig. 4b). The absorption peaks at 0.20 eV and 0.29 eV could be attributed to exciton absorptions, taking into account the structurally similar tetrahedral coordination between the fluorite-type LaH_2 and zinc-blende-type semiconductors, such as GaAs, which exhibit exciton absorption.[34] These results indicated a thickness-induced metal–semiconductor transition. The metallic behavior in the thicker films was consistent with bulk LaH_2, while the semiconducting behavior in the thinner films was observed in bulk LaH_2. Since the FWHM of the diffraction peaks did not largely depend on film thickness, the effects of micro-strain, stress, and dislocation density, which are often discussed in polycrystalline thin films, appeared to be insignificant. In addition, neither surface morphology nor composition showed dependence on thickness, suggesting that the out-of-plane lattice spacing influenced this metal–semiconductor transition.

Conclusions

In summary, we successfully grew (111)-oriented LaH_2 epitaxial thin films with varying thicknesses for the first time using reactive rf magnetron sputtering. The LaH_2 epitaxial thin films showed an increase in the out-of-plane lattice spacing with decreasing thickness, suggesting the presence of thickness-dependent lattice strain. From the electrical resistivity and optical absorption spectra, the thicker films exhibited metallic behavior similar to bulk LaH_2, while the thinner films behaved as direct band gap semiconductors. These results indicated that the modulation of out-of-plane lattice spacing *via* lattice strain induced the metal–semiconductor transition in the LaH_2 epitaxial thin films, suggesting the potential for developing of novel physical properties in rare-earth hydrides through strain engineering.

Data availability

The data supporting this article have been included as part of the ESI.†

Author contributions

S. Uramoto: investigation, validation. H. Kawasoko: conceptualization, funding acquisition, investigation, validation, supervision, writing – original draft/review and editing. S. Miyazaki: investigation, validation. T. Fukumura: funding acquisition, resources, validation, supervision, writing – review and editing.

Conflicts of interest

There are no conflicts to declare.

Acknowledgements

This study was supported by JSPS KAKENHI (21K14532).

Notes and references

1 J. N. Huiberts, R. Griessen, J. H. Rector, R. J. Wijngaarden, J. P. Dekker, D. G. de Groot and N. J. Koeman, *Nature*, 1996, **380**, 231.
2 J. W. J. Kerssemakers, S. J. van der Molen, N. J. Koeman, R. Günther and R. Griessen, *Nature*, 2000, **406**, 489.
3 V. A. Maiorov, *Opt. Spectrosc.*, 2020, **128**, 148.
4 M. Somayazulu, M. Ahart, A. K. Mishra, Z. M. Geballe, M. Baldini, Y. Meng, V. V. Struzhkin and R. J. Hemley, *Phys. Rev. Lett.*, 2019, **122**, 027001.
5 P. Drozdov, P. P. Kong, V. S. Minkov, S. P. Besedin, M. A. Kuzovnikov, S. Mozaffari, L. Balicas, F. F. Balakirev, D. E. Graf, V. B. Prakapenka, E. Greenberg, D. A. Knyazev, M. Tkacz and M. I. Eremets, *Nature*, 2019, **569**, 528.

6 K. Fukui, S. Iimura, T. Tada, S. Fujitsu, M. Sasase, H. Tamatsukuri, T. Honda, K. Ikeda, T. Otomo and H. Hosono, *Nat. Commun.*, 2019, **10**, 2578.
7 K. Fukui, S. Iimura, A. Iskandarov, T. Tada and H. Hosono, *J. Am. Chem. Soc.*, 2022, **144**, 1523.
8 W. Zhang, J. Cui, S. Wang, H. Cao, A. Wu, Y. Xia, Q. Jiang, J. Guo, T. He and P. Chen, *Nature*, 2023, **616**, 73.
9 J. Ångström, R. Johansson, T. Sarkar, M. H. Sørby, C. Zlotea, M. S. Andersson, P. Nordblad, R. H. Scheicher, U. Häussermann and M. Sahlberg, *Inorg. Chem.*, 2016, **55**, 345.
10 A. Werwein, H. Auer, L. Kuske and H. Kohlmann, *Z. Anorg. Allg. Chem.*, 2018, **644**, 1532.
11 A. Werwein, C. Benndorf, M. Bertmer, A. Franz, O. Oeckler and H. Kohlmann, *Crystals*, 2019, **9**, 193.
12 R. Shimizu, H. Oguchi and T. Hitosugi, *J. Phys. Soc. Jpn.*, 2020, **89**, 051012.
13 Y. Komatsu, R. Shimizu, M. Wilde, S. Kobayashi, Y. Sasahara, K. Nishio, K. Shigematsu, A. Ohtomo, K. Fukutani and T. Hitosugi, *Cryst. Growth Des.*, 2020, **20**, 5903.
14 N. Hasegawa, H. Kawasoko and T. Fukumura, *Chem. Lett.*, 2020, **49**, 1181.
15 Y. Komatsu, R. Shimizu, R. Sato, M. Wilde, K. Nishio, T. Katase, D. Matsumura, H. Saitoh, M. Miyauchi, J. Adelman, R. McFadden, D. Fujimoto, J. Ticknor, M. Stachura, I. McKenzie, G. Morris, W. Macfarlane, J. Sugiyama, K. Fukutani, S. Tsuneyuki and T. Hitosugi, *Chem. Mater.*, 2022, **34**, 3616.
16 T. Yamasaki, R. Takaoka, S. Iimura, J. Kim, H. Hiramatsu and H. Hosono, *ACS Appl. Mater. Interfaces*, 2022, **14**, 19766.
17 D. K. Misemer and B. N. Harmon, *Phys. Rev. B: Condens. Matter Mater. Phys.*, 1982, **26**, 5634.
18 K. Kai, K. A. Gschneidner Jr., B. J. Beaudry and D. T. Peterson, *Phys. Rev. B: Condens. Matter Mater. Phys.*, 1989, **40**, 6591.
19 S. Leyer, S. Heck, A. Kaiser, E. Dormann and R. G. Barnes, *Phys. Rev. B: Condens. Matter Mater. Phys.*, 2005, **72**, 125115.
20 H. Kim, I. Park, J. H. Shim and D. Y. Kim, *npj Comput. Mater.*, 2024, **10**, 173.
21 Y. Shi, N. Jia, J. Cai, Z. Lyu and Z. Liu, *J. Phys.: Condens. Matter*, 2022, **34**, 475303.
22 J. Shinar, B. Dehner, B. l. Beaudry and D. T. Peterson, *Phys. Rev. B: Condens. Matter Mater. Phys.*, 1988, **37**, 2066.
23 R. G. Barnes, C. T. Chang, M. Belhoul, D. R. Torgeson, B. J. Beaudry and D. T. Peterson, *J. Less-Common Met.*, 1991, **411**, 172.
24 N. Ishimatsu, R. Sasada, H. Maruyama, T. Ichikawa, H. Miyaoka, T. Kimura, M. Tsubota, Y. Kojima, T. Tsumuraya, T. Oguchi, N. Kawamura and A. Machida, *J. Phys.: Conf. Ser.*, 2009, **190**, 012070.
25 H. Mizoguchi, M. Okunaka, M. Kitano, S. Matsuishi, T. Yokoyama and H. Hosono, *Inorg. Chem.*, 2016, **55**, 8833.
26 S. Herbirowo, A. W. Pramono, H. Hendrik, H. Nugraha, V. Puspasari, A. Imaduddin, M. C. Fatah, E. Sulistiyo and A. H. Yuwono, *S. Afr. J. Chem. Eng.*, 2023, **46**, 182.
27 C. Zhang, Z.-J. Li, H. Jiang, X.-N. Hua, G.-H. Zhong and Y.-H. Su, *et al.*, *J. Alloys Compd.*, 2014, **616**, 42.
28 H. Zogg, S. Blunier, A. Fach, C. Maissen, P. Müller, S. Teodoropol, V. Meyer, G. Kostorz, A. Dommann and T. Richmond, *Phys. Rev. B: Condens. Matter Mater. Phys.*, 1994, **50**, 10801.
29 E. Boroch, K. Conder, C. R. Xiu and E. Kaldis, *J. Less Common Met*, 1989, **156**, 259.
30 J. Narayan and B. C. Larson, *J. Appl. Phys.*, 2003, **93**, 278.
31 C. E. Holley Jr., R. N. R. Mulford, F. H. Ellinger, W. C. Koehier and W. H. Zachariasen, *J. Phys. Chem.*, 1955, **59**(12), 1226.
32 W. L. Korst and J. C. Warf, *Inorg. Chem.*, 1966, **5**, 1719.
33 A. T. M. van Gogh, D. G. Nagengast, E. S. Kooij, N. J. Koeman, J. H. Rector, R. Griessen, C. F. J. Flipse and R. J. J. G. A. M. Smeets, *Phys. Rev. B: Condens. Matter Mater. Phys.*, 2001, **63**, 195105.
34 P. Y. Yu and M. Cardona, *Fundamentals of Semiconductors: Physics and Materials Properties*, Springer, Heidelberg, 4th edn, 2010.